Backscattering of underwater noise by bubble clouds

K. Sarkar and A. Prosperetti
Department of Mechanical Engineering, The Johns Hopkins University, Baltimore, Maryland 21218

(Received 10 February 1992; revised 11 January 1993; accepted 22 February 1993)

This paper is a continuation of an earlier one [Prosperetti *et al.*, J. Acoust. Soc. Am. **93**, 3117–3127 (1993)] in which the low-frequency backscattering of sound by hemispherical bubble clouds at the ocean's surface was studied. Here, clouds of various geometrical shapes (spheroids, spherical segments, cones, cylinders, ellipsoids) are considered and results in substantial agreement with the earlier ones and with the experiments of Chapman and Harris [J. Acoust. Soc. Am. **34**, 1592–1597 (1962)] are found. The implication is that the backscattering levels are not strongly dependent on the shape of the clouds, which strengthens the earlier conclusion that bubble clouds produced by breaking waves can very well be responsible for the unexpectedly high backscattering levels observed experimentally. The accuracy of the Born approximation used by others for similar problems is also examined in the light of the exact results. Significant differences are found for gas concentrations by volume of the order of 0.01% or higher. Finally, shallow nonaxisymmetric plumes are briefly considered.

PACS numbers: 43.30.Ft, 43.30.Gv

INTRODUCTION

Recently, the study of the natural mechanisms of underwater noise generation and the anomalously high backscattering levels often encountered in underwater sound propagation have stimulated an intense interest in the physics and properties of oceanic bubble clouds (Carey and Bradley, 1985; Prosperetti, 1985, 1988a, 1988b; Carey and Browning, 1988; Lu *et al.*, 1990; Yoon *et al.*, 1991; McDonald, 1991; Henyey, 1991; Lu and Prosperetti, 1993; Prosperetti *et al.*, 1993). The present paper devoted to the backscattering from clouds of various shapes is a continuation of our research activity in this area. In earlier studies we have considered bubbly layers (Lu and Prosperetti, 1993) and hemispherical clouds (Yoon *et al.*, 1991; Prosperetti *et al.*, 1993). These papers may be consulted for additional references and a more detailed discussion of the motivation and implications of this research. Here we merely stress that the mathematical model that we use for the description of the acoustic properties of bubble clouds has been found to agree remarkably well with experiment (Commander and Prosperetti, 1989; Lu *et al.*, 1990; Yoon *et al.*, 1991; Nicholas *et al.*, 1993), so that it can be used with considerable confidence in the present application.

The main result of our earlier work devoted to hemispherical bubble clouds was that the experimental backscattering data obtained by Chapman and Harris (1962) could be closely reproduced by making reasonable assumptions on the clouds' size and gas content. The purpose of the present study is to strengthen the earlier conclusions by demonstrating the relative insensitivity of those results to the detailed cloud shape. We consider several examples of axisymmetric (spheroidal and other) and nonaxisymmetric bubble clouds and hemicylindrical clouds and again find backscattering levels quite comparable to the experimental ones.

We also address the accuracy of the Born approximation in estimating scattering from bubble clouds. This part of the work is motivated by the use of that approximation in some recent studies (McDonald, 1991; Henyey, 1991). We conclude that the approximation is quite useful up to gas volume fractions of the order of $10^{-2}\%$. In the next to the last section we present an approximate treatment of nonaxisymmetric shallow clouds.

Other theoretical studies of the effect of subsurface bubbles on surface backscattering are available (see, e.g., Crowther, 1980; McDaniel and Gorman, 1982; McDaniel, 1988). However these are focused on higher frequencies and employed a theoretical formulation only suitable for exceedingly small bubble concentrations. An analysis of the relationship between those formulations and the present one is presented in a separate study (Sarkar and Prosperetti, 1993).

I. MATHEMATICAL MODEL

The mathematical model has been discussed in detail in several preceding papers (see, e.g., Commander and Prosperetti, 1989; Lu and Prosperetti, 1993; Yoon *et al.*, 1991), and so will not be repeated here. It has been shown in those papers that the governing equation for pressure perturbations in the bubbly liquid, dependent on time proportionally to $\exp i\omega t$, is a scalar Helmholtz equation with wave number κ given by

$$\kappa^2 = k^2 + \frac{4\pi\omega^2 an}{\omega_0^2 - \omega^2 + 2ib\omega}. \tag{1}$$

Here, $k=\omega/c$ (with c the speed of sound in the pure liquid), a is the equilibrium radius of the bubbles, n is the bubble number density, b is the frequency-dependent "damping constant", and ω_0 is the natural frequency of the bubble. Explicit expressions for these quantities can be found in the papers cited before. The gas volume fraction is given by

$$\beta = \tfrac{4}{3}\pi n a^3. \tag{2}$$

 0001-4966/93/063128-11$06.00

The previous expressions hold for equal-sized bubbles. Their extension to a distribution of sizes is straightforward (Commander and Prosperetti, 1989; Lu and Prosperetti, 1993) and will not be considered here. Indeed, our earlier work (Lu and Prosperetti, 1993) suggests that, at frequencies much lower than the resonance frequency of the bubbles (i.e., typically, at frequencies below several kHz), the results depend mainly on β, with the bubble radius only having a minor effect.

The pressure perturbation in the pure liquid is governed by a Helmholtz equation with wave number k. We idealize the boundary between the cloud and the pure liquid as a geometrical surface across which continuity of pressure and normal velocity are imposed. The ocean's surface is taken to be plane and the pressure perturbation is required to vanish there. This condition can be conveniently enforced by using an "image" incident wave with a suitable phase.

II. NUMERICAL METHOD FOR AXISYMMETRIC CLOUDS

In our earlier work on hemispherical clouds we made use of spherical polar coordinates and separation of variables. A similar approach could be followed for hemispheroidal clouds (see, e.g., Yeh, 1967). However, this would lead to complicated functions with a complex argument and the results, although analytical, would not be particularly transparent. For this reason we have preferred to use a version of the T-matrix method (see, e.g., Waterman, 1969; Visscher, 1980a, 1980b). In this way, we are also able to treat other shapes for which no separable coordinate system is available. To reduce the computing requirements we confine our study to axisymmetric shapes. As an example of more general shapes, we consider hemicylindrical clouds in Secs. IV and V below and a simple model of nonaxisymmetric "shallow" clouds in Sec. VII. An extensive literature is available on the T-matrix method [in particular, see Visscher (1980a) whose notation is followed here] and only a very brief description of the procedure will be sufficient. The basic difference with the case of hemispherical clouds of Prosperetti *et al.* (1993) is that, since the boundary does not conform to a coordinate surface, all the partial wave components are coupled and must be determined simultaneously. Mathematically, this circumstance leads to an algebraic system the matrix of which is full rather than diagonal as in the previous case.

We write the pressure perturbation p as the superposition of the incident field $p^{\rm inc}$, the field $p^{\rm ref}$ specularly reflected from the plane pressure-release surface, and the field $p^{\rm scat}$ scattered by the bubble cloud,

$$p(\mathbf{x})=p^{\rm inc}(\mathbf{x})+p^{\rm ref}(\mathbf{x})+p^{\rm scat}(\mathbf{x}). \tag{3}$$

The first two terms are expanded in a complete orthonormal set of functions $\{\tilde{\phi}^s(\mathbf{x})\}$ (where the index s is shorthand for the set of indices required for a complete specification)

$$p^{\rm inc}(\mathbf{x})+p^{\rm ref}(\mathbf{x})=\sum_s d_s\tilde{\phi}_s(\mathbf{x}). \tag{4}$$

Since we only consider plane waves, we take

$$\tilde{\phi}_s\equiv\tilde{\phi}_{lm}=j_l(kr)\,Y_{lm}(\theta,\varphi), \tag{5}$$

where j_l is a spherical Bessel function of the first kind, Y_{lm} is a spherical harmonic, and θ and φ are the polar angles defined in the standard way. The radial coordinate r is measured from the center of the "footprint" of the cloud on the ocean's surface. We choose a coordinate system such that the polar axis is orthogonal to the ocean surface and directed upward. The plane of incidence is the plane $\varphi=0$. We take the original incident wave to be plane with unit amplitude and its wave vector to make an angle η (grazing angle) with the $z=0$ plane. We then have

$$p^{\rm inc}=\exp(-i\mathbf{k}\cdot\mathbf{x}),\quad p^{\rm ref}=-\exp(-i\mathbf{k}_r\cdot\mathbf{x}), \tag{6}$$

with $\mathbf{k}=(k\cos\eta,0,k\sin\eta)$, $\mathbf{k}_r=(k\cos\eta,0,-k\sin\eta)$. Then the coefficients d_s are given by

$$d_{lm}=4\pi[1-(-1)^{l+m}](-i)^l\bar{Y}_{lm}(\pi/2-\eta,0), \tag{7}$$

$$d_{l,-m}=4\pi[1-(-1)^{l+m}](-i)^l(-1)^mY_{lm}(\pi/2-\eta,0), \tag{8}$$

where the overline denotes the complex conjugate.

The scattered wave is similarly expanded as

$$p^{\rm scat}(\mathbf{x})=\sum_{s'}a_{s'}\phi^+_{s'}(\mathbf{x}), \tag{9}$$

where, in view of the radiation condition, we take

$$\phi^+_{s'}=\phi^+_{l'm'}=h^{(2)}_{l'}(kr)\,Y_{l'm'}(\theta,\varphi), \tag{10}$$

with $h^{(2)}_{l'}$ a spherical Hankel function of the second kind. At a large distance from the scatterer, using the asymptotic properties of $h^{(2)}_l$, we have

$$p^{\rm scat}=(R_c/r)f_*(\theta,\varphi)\exp(-ikr), \tag{11}$$

where R_c is the radius of the trace of the cloud on the ocean's surface and f_* is the dimensionless scattering amplitude given by

$$f_*(\theta,\varphi)=\frac{1}{kR_c}\sum_{lm}a_{lm}i^{l+1}Y_{lm}(\theta,\varphi). \tag{12}$$

The final expression for the dimensionless scattering cross section is

$$\sigma_*(\theta,\varphi)=(1/\pi)\,|f_*(\theta,\varphi)|^2. \tag{13}$$

Physically, σ_* represents the scattering cross section nondimensionalized by the area of the "footprint" of the cloud on the surface.

Inside the scattering target we express the perturbation pressure as

$$p^{\rm cloud}(\mathbf{x})=\sum_s b_s\tilde{\psi}_s(\mathbf{x}), \tag{14}$$

where regularity of $\tilde{\psi}_s$ at the origin makes it identical to $\tilde{\phi}_s$, with k replaced by the effective wave number κ appropriate to the bubbly mixture inside the scatterer.

The objective of the calculation is to determine the amplitudes a_s's and b_s's satisfying, on the cloud's surface, the conditions of continuity of pressure,

$$p-p^{\text{cloud}}=0, \tag{15}$$

and normal velocity

$$\mathbf{n}\cdot[\nabla p-\nabla p^{\text{cloud}}]=0. \tag{16}$$

These conditions are imposed by projection on a complete system of functions $\{f_s\}$ and $\{g_s\}$, respectively. By taking scalar products we find

$$\sum_{s'}[d_{s'}(f_s,\tilde{\phi}_{s'})+a_{s'}(f_s,\phi_{s'}^{+})-b_{s'}(f_s,\tilde{\psi}_{s'})]=0, \tag{17}$$

and

$$\sum_{s'}[d_{s'}(g_s,\mathbf{n}\cdot\nabla\tilde{\phi}_{s'})+a_{s'}(g_s,\mathbf{n}\cdot\nabla\phi_{s'}^{+}) -b_{s'}(g_s,\mathbf{n}\cdot\nabla\tilde{\psi}_{s'})]=0, \tag{18}$$

where $(\cdot,\cdot)$ denotes the scalar product

$$(u,v)=\int_{\Sigma}\bar{u}v\,d\Sigma. \tag{19}$$

The integration is extended over the surface Σ consisting of the surface of the actual cloud and of its image in the plane. This definition can be understood by noting that, as formulated, the present scattering process is equivalent to the superposition of the scattering by an object bounded by the surface Σ just defined, of the actual beam and an "image" beam with opposite phase, both propagating in unbounded space.

Upon introducing infinite matrices Q', Q, $\tilde{Q}$, R'', R', and $\tilde{R}'$, with elements given by

$$Q'_{s,s'}=(f_s,\tilde{\psi}_{s'}),\quad Q_{s,s'}=(f_s,\phi_{s'}^{+}),\quad \tilde{Q}_{s,s'}=(f_s,\tilde{\phi}_{s'}), \tag{20}$$

$$R''_{s,s'}=(g_s,\mathbf{n}\cdot\nabla\tilde{\psi}_{s'}),\quad (R'^{\dagger})_{s,s'}=(g_s,\mathbf{n}\cdot\nabla\phi_{s'}^{+}),$$

$$\tilde{R}'_{s,s'}=(g_s,\mathbf{n}\cdot\nabla\tilde{\phi}_{s'}), \tag{21}$$

where the symbol $\dagger$ indicates the adjoint, and vectors $\mathbf{a}=\{a_s\}$, $\mathbf{b}=\{b_s\}$, $\mathbf{d}=\{d_s\}$, the preceding system of equations is readily seen to lead to the following formal solution for the vector $\mathbf{a}$ of scattering amplitudes

$$\mathbf{a}=-(Q-Q'R''^{-1}R'^{\dagger})^{-1}\times(\tilde{Q}-Q'R''^{-1}\tilde{R}')\mathbf{d}\equiv T\mathbf{d}. \tag{22}$$

The choice of the complete system $\{f_s\}$, $\{g_s\}$ would be immaterial if all the terms in the expansions were retained. Since, however, one is forced to deal with truncated forms of the previous relations, it is important to use functions exhibiting fast convergence properties. This question has been examined by Visscher (1980a) who suggests the choice

$$f_s=\phi_s^{+},\quad g_s=\mathbf{n}\cdot\nabla\tilde{\psi}_s, \tag{23}$$

to which we adhere. It may be shown that, due to the axial symmetry of the scatterer, the matrices defined in (20), (21) take a block-diagonal form (Visscher, 1980a). Each block corresponds to a different value of the index m and the elements of the block depend on the indices l, l'.

The numerical implementation of the previous scheme is not without difficulties. While we have been able to resolve some of them to the extent needed for the purposes of the present paper, we cannot claim complete success. The problems are due to the slowness of convergence of the expansion and to the increasing ill-conditioning of the matrices with higher-order truncation. This circumstance makes it difficult to retain a number of terms sufficient for high accuracy. In addition to the functions (23), we have also used the conventional spherical harmonics but found an even slower convergence. To make sure that the difficulties encountered were not due to coding errors we have obtained analytical results for spheroids of small eccentricity by domain perturbation and have checked that the code reproduced them exactly.

In the calculations we have retained all the terms with $l\leqslant l_{\max}=18$. The surface integrations needed for the calculation of the scalar products in (20), (21) have been performed numerically by the 60-point Gauss–Legendre quadrature formula. For some cases we have used up to 100 points with negligible differences. The solution of the system (22) was effected with the IMSL routine DLINCG. The condition number of the matrices was large enough that the routine issued a warning message. To make sure that the solution found was, nevertheless, accurate, we checked by direct substitution that the equations of the system (22) were satisfied, and we plotted the two sides of Eqs. (15) and (16) as a function of θ for fixed φ to inspect visually the magnitude of the error. Both tests were satisfactory. If $l_{\max}$ was reduced sufficiently to avoid the warning message, it was found that the continuity requirements (15) and (16) were only poorly satisfied. On the other hand, a bigger value for $l_{\max}$ caused a degradation in the accuracy of the solution. In general the condition number was worse at the lower frequencies, and convergence slower the greater the difference between the cloud's radius and depth.

After all the tests carried out on the program and the numerical results we are satisfied that the code worked correctly and that the remaining relatively minor inaccuracies (to be discussed in the following section) are intrinsic to the method in the present application.

III. NUMERICAL RESULTS: AXISYMMETRIC CLOUDS

The backscattering strength Σ_B is defined by (see, e.g., Urick, 1967)

$$\Sigma_B=R^2I_s/I_i\,\Delta A, \tag{24}$$

where I_i is the sound intensity of the incident wave, I_s is the intensity of the wave scattered in the backward direction, ΔA is the ensonified area, and R is the distance between ΔA and the receiver. The definition presupposes that $\Delta A\ll R^2$. From (12) and (13) we find

$$\Sigma_B=\frac{\pi R_c^2}{\Delta A}\,\sigma_*\left(\frac{\pi}{2}+\eta,\pi\right). \tag{25}$$

The ratio in the right-hand side of this equation can be approximated by the fraction W of the ocean's surface cov-

ered by whitecaps, which is known experimentally. An empirical correlation for this quantity is (Monahan and O'Muircheartaigh, 1980)

$$W=3.86\times10^{-6}U^{3.41}, \tag{26}$$

where U, expressed in m/s, is the wind speed. For example, at wind speeds of 5, 10, and 15 m/s, this relation gives $W=9.33\times10^{-4}$, 9.92×10^{-3}, and 0.040, respectively.

Usually, the backscattering strength is expressed in dB according to the definition

$$S(\eta)=10\log_{10}\Sigma_B$$
$$=10\log_{10}\sigma_*(\pi/2+\eta,\pi)+10\log_{10}W. \tag{27}$$

This is the quantity reported by Chapman and Harris (1962) who fitted their data to ±3 dB with the expression

$$S(\eta)=3.3b\log_{10}(\eta/30^\circ)-42.4\log_{10}b+2.6, \tag{28}$$

where

$$b=107.5(U\nu^{1/3})^{-0.58}, \tag{29}$$

with $\nu=\omega/2\pi$ is the sound frequency. This correlation was obtained on the basis of data over the range $0.4\leqslant\nu\leqslant6.4$ kHz, $0\leqslant U\leqslant15.4$ m/s, $3^\circ\leqslant\eta\leqslant40^\circ$, although not the entire ranges were covered for all values of the variables. The functional dependence of (27) and (28) upon the wind velocity U is somewhat different. However, it is found numerically that this difference is well within ±3 dB's for the range $5\leqslant U\leqslant25$ m/s, $0.1\leqslant\nu\leqslant2$ kHz, $5^\circ\leqslant\eta\leqslant30^\circ$.

We now compare the predictions of our theory with the Chapman–Harris correlation for bubble clouds of different shapes. We take the bubbles to be all equal and uniformly distributed. The effects of a non-uniform distribution of bubbles were considered in Prosperetti *et al.* (1993) for hemispherical clouds and found to be of secondary importance for the range of volume fractions and frequencies of present concern. The equilibrium radius of the bubbles is taken as 1 mm and the gas volume fraction in the cloud as 1%. In our previous work (Prosperetti *et al.*, 1993) we have studied the effect of these quantities and have found it to be small for the frequency range between 0.2 and 2 kHz to which we limit our considerations. We also only present results for a representative value of the grazing angle, $\eta=20^\circ$, and of the radius of the cloud's footprint on the ocean's surface, $R_c=0.5$ m. Other values of these quantities are considered in Prosperetti *et al.* (1993) for hemispherical clouds, and a similar dependence is expected for the shapes studied here. In the figures the right vertical scale is the backscattering strength for a windspeed of 10 m/s. The present predictions for $U=5$, 15, and 20 m/s can be obtained by subtracting 10.3 dB or adding 6.00 and 10.3 dB, respectively. The gray area indicates the empirical ±3 dB error band around the correlation (28).

In Fig. 1 results for the scattering from a prolate spheroid with depth d larger than the radius R_c of its footprint on the ocean's surface are shown. The solid line corresponds to the spherical case $d/R_c=1$ considered in Prosperetti *et al.* (1993). The dotted line is for a spheroid with

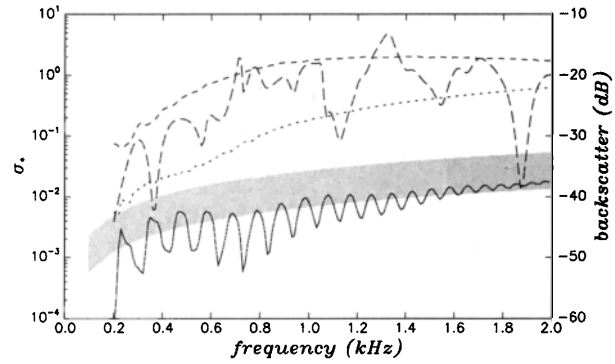

FIG. 1. Dimensionless backscattering cross section for prolate spheroidal bubble clouds (left scale) and backscattering strength for a 10-m/s wind (right scale) for a 20° grazing angle. At this wind speed the fraction of the ocean surface covered by bubble clouds is estimated to be slightly less than 1%. The gray band indicates Chapman and Harris's (1962) data ±3 dB. The radius of the cloud's footprint on the ocean surface is $R_c=0.5$ m and the vertical extent of the cloud below the surface is $d/R_c=1$ (solid line), $d/R_c=2$ (dotted line), and $d/R_c=5$ (dashed lines). The radius of the bubbles is 1 mm and the air volume fraction in the cloud is 1% for the solid, dotted, and smooth dashed lines and 0.01% for the strongly oscillating dashed line.

$d/R_c=2$ (i.e., $d=1$ m), while both of the dashed lines are for $d/R_c=5$, the smoother one for a volume fraction of 1% and the oscillating one for 10^{-2}%, which is more realistic for a depth of $d/R_c=5$. Clearly, the maximum depth reached by the bubbles has a very strong effect. The experimental results (28), which are fairly well approximated by the hemispherical cloud, can be more closely reproduced with a very slight increase in the cloud's depth.

The pattern of oscillations exhibited by the results for the hemispherical cloud is conspicuously absent from the 1% spheroidal cloud results. We attribute this to the unsatisfactory performance of the numerical method used, as described in the previous section. We have found that, as the eccentricity of the spheroid was increased from zero, the oscillations tended to become weaker and then nearly disappear. As was discussed in Prosperetti *et al.* (1993), these oscillations are not present in the experimental data that in fact average over many clouds, and are therefore not essential for the present purposes. However their absence does indicate an insufficiency of the numerical technique. We believe however that the relatively smooth curve found numerically represents the basic trend of the actual system's behavior as its position was little affected by the choice of $l_{\max}$ or the use of one or another family of basis functions in the scalar products (23). Hence, while the present results do not exhibit a large degree of detail, they appear to be sufficiently accurate for the present purposes. It appears that the numerical problems are mitigated in the case of the smaller volume fraction. For small β the imaginary part of the wave number in the cloud (1) is smaller and possibly this feature aids in the numerical resolution of the scattering cross section.

The case of oblate spheroids for which $d/R_c<1$ is considered in Fig. 2 where the solid line is again for the spherical cloud while the other ones correspond, in descending order, to $d/R_c=0.75$ and 0.5. Results for another shape

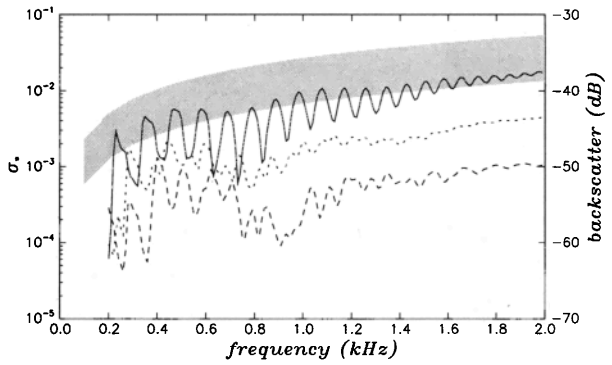

FIG. 2. Dimensionless backscattering cross section for oblate spheroidal bubble clouds (left scale) and backscattering strength for a 10-m/s wind (right scale) for a 20° grazing angle. The gray band indicates Chapman and Harris's (1962) data ±3 dB. The radius of the cloud's footprint on the ocean surface is R_c=0.5 m and the vertical extent of the cloud below the surface is d/R_c=1 (solid line), d/R_c=0.75 (dotted line), and d/R_c =0.5 (dashes). The radius of the bubbles is 1 mm and the air volume fraction in the cloud is 1%.

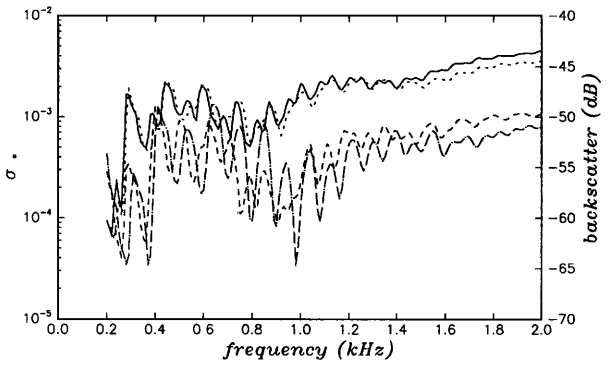

FIG. 4. Comparison of dimensionless backscattering cross sections (left scale) and backscattering strengths in a 10-m/s wind (right scale) for spheroidal (solid and dashed lines) and spherical-segment (dotted and dash-and-dotted lines) bubble clouds. The radius of the footprint on the surface is R_c=0.5 m. The upper pair of curves is for d/R_c=0.75, the lower pair for d/R_c=0.5. Note the relative insensitivity of the results to the cloud's shape.

with $d/R_c<1$, a spherical segment, are shown in Fig. 3 for the same values of d/R_c. The levels in the two figures are comparable, which seems to indicate a relative insensitivity to the detailed shape of the cloud, the parameter of greatest importance being the depth of submergence. This point is examined in greater detail in Fig. 4 where the spheroid and spherical-segment results are compared for the two cases d/R_c=0.75 (upper pair of curves) and 0.5.

A third axisymmetric shape that we consider (Fig. 5) is a vertical cone with the base on the ocean's surface and the apex at a depth of—in ascending order—d/R_c=0.25, 0.5, 1, 2, and 5. As in the case of the prolate spheroidal shape, the levels become comparable with the experimental ones (28) for d/R_c somewhere between 1 and 2 (i.e., d between 0.5 and 1 m). Of course this conclusion depends on the assumed radius of the footprint as shown in Prosperetti *et al.* (1993). The magnitude of the effect is worth stressing: bubble plumes with a volume of the order of a fraction of 1-m^3 covering less than 1% of the ocean's surface are amply sufficient to account for the observed backscattering levels.

IV. CYLINDRICAL CLOUDS

As a simple example of clouds that exhibit a strong difference between their extent along the surface and their depth we consider now the case of hemicylindrical shapes. In this case the cylindrical coordinate system conveniently furnishes analytical results and there is no need for the numerical method previously described.

We take the horizontal axis of the cylinder as the y axis of a cylindrical coordinate system. The z axis is vertically upward and the free surface coincides with the xy plane. The radius of the cylinder is denoted by R_c. As before we set

$$p^{\text{inc}}+p^{\text{ref}}=\exp(-i\mathbf{k}\cdot\mathbf{x})-\exp(-i\mathbf{k}_r\cdot\mathbf{x}), \tag{30}$$

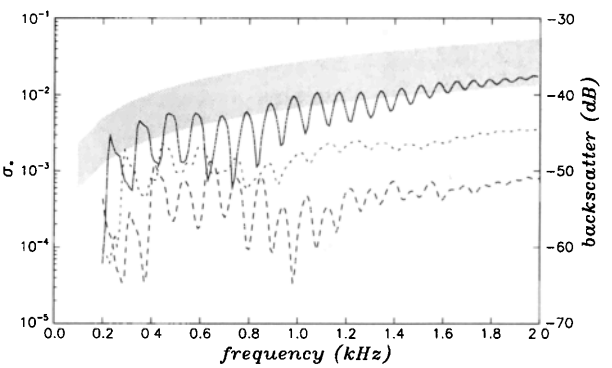

FIG. 3. Dimensionless backscattering cross section for a bubble cloud in the form of a spherical segment (left scale) and backscattering strength for a 10-m/s wind (right scale) for a 20° grazing angle. The gray band indicates Chapman and Harris's (1962) data ±3 dB. The radius of the cloud's footprint on the ocean surface is R_c=0.5 m and the vertical extent of the cloud below the surface is d/R_c=1 (solid line), d/R_c=0.75 (dotted line), and d/R_c=0.5 (dashes). The radius of the bubbles is 1 mm and the air volume fraction in the cloud is 1%.

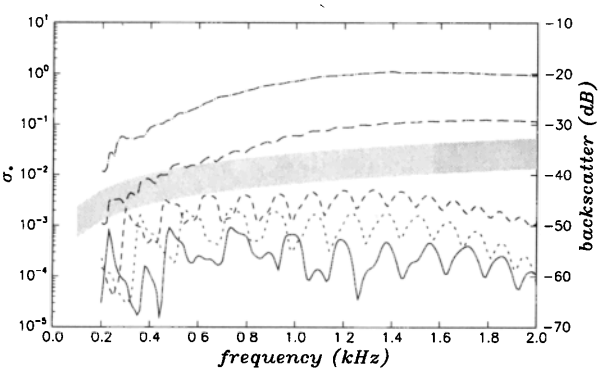

FIG. 5. Dimensionless backscattering cross section for bubble clouds in the form of a right circular cone (left scale) and backscattering strength for a 10-m/s wind (right scale) for a 20° grazing angle. The gray band indicates Chapman and Harris's (1962) data ±3 dB. The radius of the cloud's footprint on the ocean surface is R_c=0.5 m. The vertical extent of the cloud below the surface is, in ascending order, d/R_c=0.5 (solid line), d/R_c=0.75 (dotted line), and d/R_c=1 (short dashes), d/R_c=2 (long dashes), and d/R_c=5 (dashes and dots). The radius of the bubbles is 1 mm and the air volume fraction in the cloud is 1%.

where $\mathbf{k}=(k_x,k_y,k_z)$ and $\mathbf{k}_r=(k_x,k_y,-k_z)$ are the wave numbers of the incident and specularly reflected waves. If η is, as before, the grazing angle [i.e., the angle that the vector $\mathbf{k}$ makes with the (x,y) plane], and γ the angle that the projection of $\mathbf{k}$ on the (x,y) plane makes with the x axis, we have

$$k_x=k\cos\eta\cos\gamma,\quad k_y=k\cos\eta\sin\gamma,\quad k_z=k\sin\eta. \tag{31}$$

To write the following formulas more compactly it is useful to introduce the auxiliary quantities $\hat{k}$, $\hat{\eta}$ defined by

$$\hat{k}=\sqrt{k_x^2+k_z^2}=k\sqrt{\cos^2\eta\cos^2\gamma+\sin^2\eta},$$
$$k_x=\hat{k}\cos\hat{\eta},\quad k_z=\hat{k}\sin\hat{\eta}. \tag{32}$$

Regularity at the origin and the radiation condition at infinity demand that the perturbation pressure field inside the cloud and the scattered wave have, respectively, the form

$$p^{\text{cloud}}=e^{-ik_y y}\sum_{n=1}^{\infty}A_nJ_n(\varpi\sqrt{\kappa^2-k_y^2})\sin n\vartheta, \tag{33}$$

$$p^{\text{scat}}=e^{-ik_y y}\sum_{n=1}^{\infty}B_nH_n^{(2)}(\hat{k}\varpi)\sin n\vartheta, \tag{34}$$

where ϖ, ϑ are the standard radial and angular variables of the cylindrical coordinate system and the continuity requirement of pressure has been partially anticipated in writing the y dependence.

From the continuity of pressure on the interface $\varpi=R_c$ we obtain

$$B_nH_n^{(2)}(v)-A_nJ_n(u)=-4(-i)^nJ_n(v)\sin n\hat{\eta}, \tag{35}$$

and from the continuity of velocity

$$B_nvH_n'^{(2)}(v)-A_nuJ_n'(u)=-4(-i)^nvJ_n'(v)\sin n\hat{\eta}, \tag{36}$$

where

$$u=\sqrt{\kappa^2-k_y^2}R_c,\quad v=\hat{k}R_c. \tag{37}$$

The amplitudes of the partial scattered waves found from (35) and (36) are

$$B_n=-4(-i)^nT_n(u,v)\sin n\hat{\eta}, \tag{38}$$

where

$$T_n=\frac{u[J_{n-1}(u)/J_n(u)]-v[J_{n-1}(v)/J_n(v)]}{u[J_{n-1}(u)/J_n(u)]-v[H_{n-1}^{(2)}(v)/H_n^{(2)}(v)]}\frac{J_n(v)}{H_n^{(2)}(v)}. \tag{39}$$

We define a dimensionless scattering amplitude f_* of the bubble cloud similarly to (12) by writing that, as $r\to\infty$, p^{scat} approaches

$$p^{\text{scat}}\to\sqrt{R_c/\varpi}\exp(-ik_y y-i\hat{k}\varpi)f_*(\theta). \tag{40}$$

By using the asymptotic properties of $H_n^{(2)}$ we find

$$f_*(\vartheta)=-\frac{4(1+i)}{\sqrt{\pi R_c\hat{k}}}\sum_{n=1}^{\infty}T_n(u,v)\sin n\vartheta\sin n\hat{\eta}. \tag{41}$$

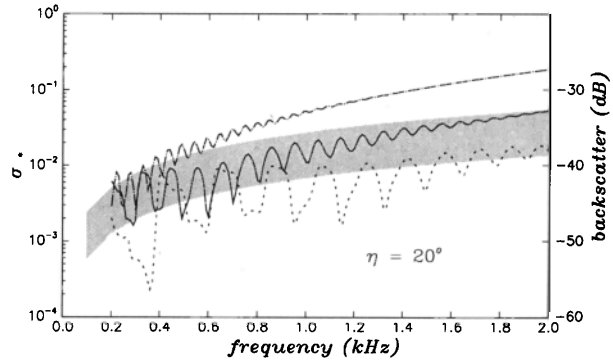

FIG. 6. Two-dimensional backscattering cross section (42) from hemicylindrical bubble clouds (left scale) and backscattering strength for a 10-m/s wind (right scale) for a 20° grazing angle. The gray band indicates Chapman and Harris's (1962) data ±3 dB. The cloud radii are 0.25, 0.5, and 1 m for the dotted, solid, and dashed-and-dotted lines. The radius of the bubbles is 1 mm and the air volume fraction in the cloud is 1%.

The dimensionless differential cross section σ_* is related to f_* by

$$\sigma_*(\vartheta)=\tfrac{1}{2}|f_*(\vartheta)|^2. \tag{42}$$

Clearly the definition (24) of backscattering strength used before is not suitable for the present situation. By analogy we propose the definition

$$\Sigma_B\simeq\frac{R}{\Delta l}\frac{I_s}{I_i}, \tag{43}$$

where Δl is the width of the ensonified region. It may be noted that a similar expression would be found from (24) by considering a situation in which the source is at a distance R from the axis of the cylinder and the ensonified region is rectangular with length R parallel and width Δl orthogonal to the cloud.

It should also be noted that, since there is no mechanism for the reversal of the component of $\mathbf{k}$ in the y direction, there can be no truly backscattered wave unless $k_y=0$, i.e., $\gamma=0$, $\hat{\eta}=\eta$. Restricting ourselves to this case, with the definition (43), we have from (42)

$$\Sigma_B=\frac{2R_c}{\Delta l}\sigma_*(\eta-\pi). \tag{44}$$

As before we take $2R_c/\Delta l=W$ to find the same relation (28) for the backscattering strength in dB.

V. NUMERICAL RESULTS: CYLINDRICAL CLOUDS

As before we consider a reference case consisting of clouds with a gas volume fraction of 1% and bubbles with a 1-mm radius. For the consideration of backscattering, as explained before, we also take the incident plane wave propagating perpendicularly to the axis of the cylinder so that $\gamma=0$.

Figures 6–8 show the dimensionless cross section (42) and backscattering strength in dB for grazing angles of 20°, 30°, and 80°. For the first two cases the gray band indicates the Chapman–Harris result. In the figures the dotted line is for $R_c=0.25$ m, the solid line for $R_c=0.5$ m, and the dash-

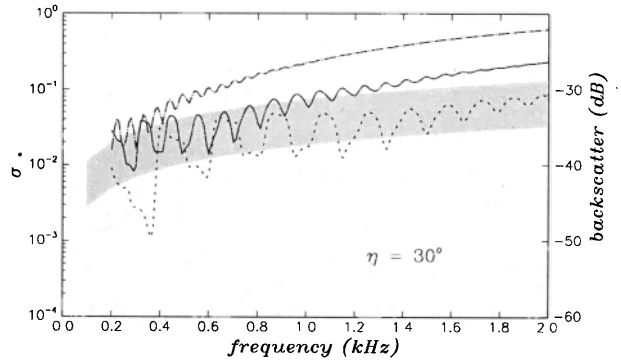

FIG. 7. Two-dimensional backscattering cross section (42) from hemicylindrical bubble clouds (left scale) and backscattering strength for a 10-m/s wind (right scale) for a 30° grazing angle. The gray band indicates Chapman and Harris's (1962) data ±3 dB. The cloud radii are 0.25, 0.5, and 1 m for the dotted, solid, and dashed-and-dotted lines. The radius of the bubbles is 1 mm and the air volume fraction in the cloud is 1%.

and-dotted line for $R_c=1$ m. Again a general compatibility of the calculated results and the data is observed, not only in level, but also in the dependence on frequency. The results display the oscillatory structure already encountered in the hemispherical case.

VI. VALIDITY OF BORN APPROXIMATION

Recently several investigators (McDonald, 1991; Henyey, 1991) have made use of the Born approximation to estimate the backscattering from bubble plumes. Since we possess exact solutions, it is interesting to compare them with the approximate ones to establish their range of validity. We shall do this for the case of hemispherical clouds that was treated in Prosperetti *et al.* (1993).

To derive the approximation we proceed in the usual way by rewriting the Helmholtz equation as

$$(\nabla^2+k^2)p=(k^2-\kappa^2)p, \tag{45}$$

with the understanding that the right-hand side vanishes in the pure liquid. [Alternatively, we can consider the bubble number density n in Eq. (1) to be a function of position

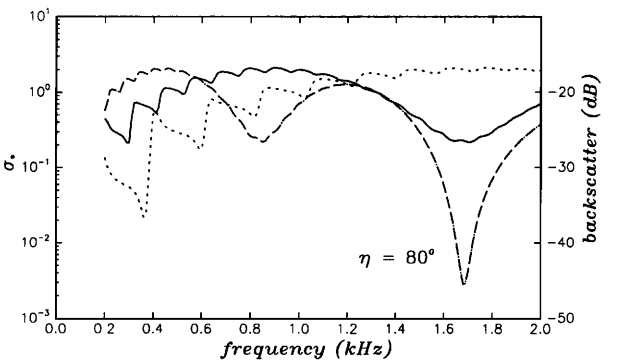

FIG. 8. Two-dimensional backscattering cross section (42) from hemicylindrical bubble clouds (left scale) and backscattering strength for a 10-m/s wind (right scale) for a 80° grazing angle. The cloud radii are 0.25, 0.5, and 1 m for the dotted, solid, and dashed-and-dotted lines. The radius of the bubbles is 1 mm and the air volume fraction in the cloud is 1%.

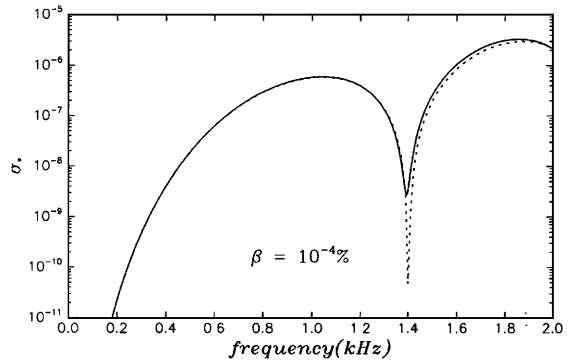

FIG. 9. Comparison of the Born approximation (49) (dotted line) with the exact result (solid line) for the dimensionless backscattering cross section from a hemispherical bubble cloud with a radius of 0.5 m. The grazing angle is 20° and the gas volume fraction $10^{-4}\%$.

that vanishes in the pure liquid.] Equation (45) can be transformed into an integral relation by use of the Green's function $G(\mathbf{x},\mathbf{x}')$ appropriate to the present case of a pressure-release plane boundary,

$$G(\mathbf{x},\mathbf{x}')=\frac{\exp(-ik|\mathbf{x}-\mathbf{x}'|)}{4\pi|\mathbf{x}-\mathbf{x}'|}-\frac{\exp(-ik|\mathbf{x}-\mathbf{x}'_r|)}{4\pi|\mathbf{x}-\mathbf{x}'_r|}, \tag{46}$$

where $\mathbf{x}'_r$ is the point $\mathbf{x}'$ "reflected" in the plane boundary. The approximation consists of writing in the integral, in place of the exact field solution of (45), the incident field plus the specularly reflected wave

$$p^{\text{inc}}+p^{\text{ref}}=\exp(-i\mathbf{k}\cdot\mathbf{x})-\exp(-i\mathbf{k}_r\cdot\mathbf{x}), \tag{47}$$

where $\mathbf{k}_r$ is as in (6). By using the definition (13) of the dimensionless scattering amplitude and by exploiting the assumed axial symmetry of the cloud, we readily find

$$f_{B*}=\frac{\kappa^2-k^2}{R_c}\int_{\pi/2}^{\pi}d\theta\sin\theta\int_0^{R(\theta)}dr \times r^2[1-\cos(2k_\perp r\cos\theta)]J_0(2k_\parallel r\sin\theta), \tag{48}$$

where $R(\theta)$ is the trace of the cloud's contour on the meridian plane in plane polar coordinates, $k_\perp=k\sin\eta$, and $k_\parallel=k\cos\eta$.

For a hemispherical cloud the integral can be calculated exactly to find

$$f_{B*}=\frac{\kappa^2-k^2}{8R_ck^3}\left(\frac{k^3}{k_\parallel^3}F(2k_\parallel R_c)-F(2kR_c)\right), \tag{49}$$

where $F(z)=\sin z-z\cos z$.

The backscattering strength obtained from this result is compared with the exact one of Prosperetti *et al.* (1993) in Figs. 9 to 12, all for $R_c=0.5$ m, $\eta=20°$, and bubbles with an equilibrium radius of 1 mm. The figures compare σ_* as a function of frequency for increasing values of the gas volume fraction β. The solid lines are the exact results and the dotted lines the Born approximation. As could be anticipated, the approximation is better away from resonances. Even at a volume fraction as low as $10^{-4}\%$ (Fig. 9), the error in the neighborhood of the lowest resonance

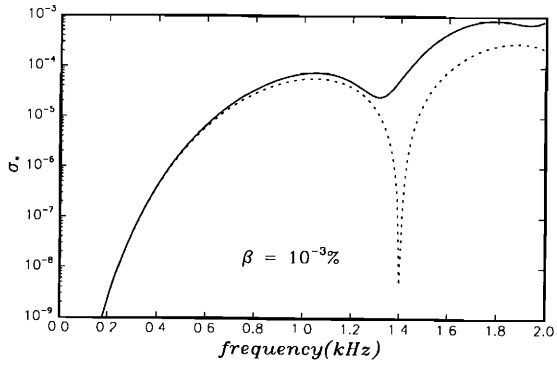

FIG. 10. Comparison of the Born approximation (49) (dotted line) with the exact result (solid line) for the dimensionless backscattering cross section from a hemispherical bubble cloud with a radius of 0.5 m. The grazing angle is 20° and the gas volume fraction 10^{-3}%.

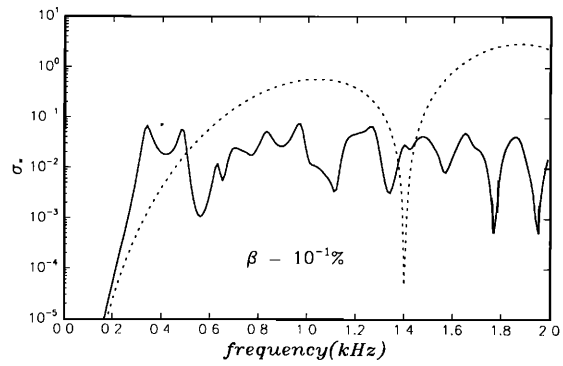

FIG. 12. Comparison of the Born approximation (49) (dotted line) with the exact result (solid line) for the dimensionless backscattering cross section from a hemispherical bubble cloud with a radius of 0.5 m. The grazing angle is 20° and the gas volume fraction 0.1%.

of the cloud is about two orders of magnitude. At $\beta=10^{-3}$% (Fig. 10) a significant error persists above the fundamental resonance, and at 10^{-2}% (Fig. 11) the approximation fails except at very low frequency. At the still pretty small volume fraction of 0.1%, there is little resemblance between the Born approximation and the exact result (Fig. 12).

For more general cases it is not easy or possible to obtain closed-form solutions such as (49). A low-frequency approximation can however easily be derived from (48) by keeping the first two terms of the Taylor series expansion of the cosine and approximating J_0 by 1. In this way, and passing to Cartesian coordinates, one finds

$$f_{B*}=2k_\perp^2\,\frac{k^2-\kappa^2}{R_c}\int_{\text{cloud}} xz^2\,dz\,dx, \tag{50}$$

where the integral is over the trace of the cloud in the meridian plane. This form is convenient to derive the scaling of the scattering amplitude with the dimensions of the cloud. By setting $x=R_c\xi$, $z=d\zeta$ we have

$$f_{B*}=k_\perp^2\,(k^2-\kappa^2)R_c d^3\left(2\int\int \xi\zeta^2\,d\xi\,d\zeta\right). \tag{51}$$

The quantity in parenthesis is a pure number (equal, e.g., to 2/15 for hemispherical and spheroidal clouds, and to 1/30 for conical clouds), so that this relation predicts the scattering amplitude to increase according to the third power of the cloud's depth and, therefore, the backscattering cross section according to the sixth power. We test this prediction with the numerical results of Sec. III for spheroidal and conical clouds in Figs. 13 and 14 respectively for the same conditions as before and for $\nu=0.1$ kHz. Here the dotted lines are for $\beta=10^{-4}$%, the dashed lines for $\beta=10^{-2}$%, and the dash-and-dotted lines for $\beta=1$%. The solid lines are a graph of (51). For the two lower volume fraction cases the approximation (51) is seen to work well up to a depth of the order of 1 m. There is a slight discrepancy at the lower depths of immersion which is probably due to the numerical difficulties mentioned above which are particularly acute when the ratio R_c/d is very different from 1. The higher volume-fraction case shows a faster growth with d than predicted by (51) and then a flattening out for still greater depths. It may be noted that, for these examples, the parameter kR_c, on the smallness of which the approximation of (48) by (51) relies, has the value 0.212.

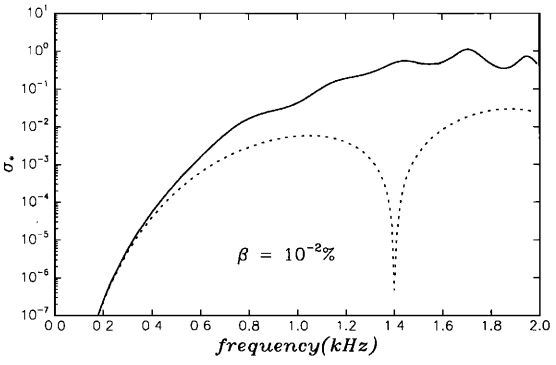

FIG. 11. Comparison of the Born approximation (49) (dotted line) with the exact result (solid line) for the dimensionless backscattering cross section from a hemispherical bubble cloud with a radius of 0.5 m. The grazing angle is 20° and the gas volume fraction 10^{-2}%.

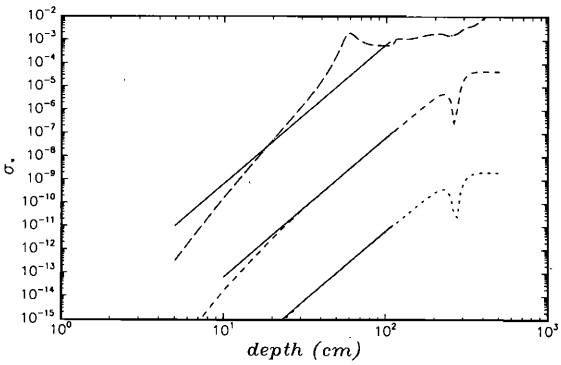

FIG. 13. Dimensionless backscattering cross section at 0.1 kHz for spheroidal clouds as a function of the cloud's depth d. The solid lines are the Born low-frequency approximation (51) and the broken lines the numerical results according to the procedure of Sec. II. The gas volume fractions are, in ascending order, 10^{-4}%, 10^{-2}%, and 1%. The grazing angle is 20°.

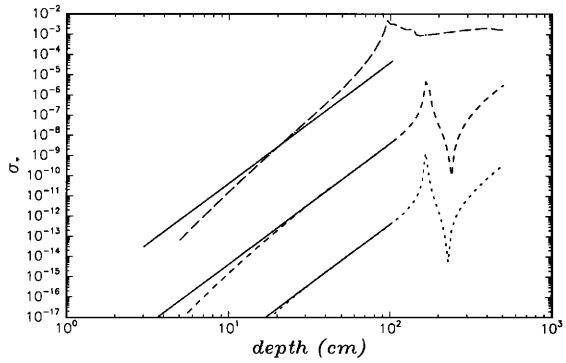

FIG. 14. Dimensionless backscattering cross section at 0.1 kHz for conical clouds as a function of the cloud's depth d. The solid lines are the Born low-frequency approximation (51) and the broken lines the numerical results according to the procedure of Sec. II. The gas volume fractions are, in ascending order, 10^{-4}%, 10^{-2}%, and 1%. The grazing angle is 20°.

VII. "SHALLOW" CLOUDS

A nonaxisymmetric case that can be simply treated is that in which the maximum depth d of the bubble cloud is much less than its horizontal dimensions and, furthermore, $kd \ll 1$. Even in the axisymmetric case it is worth while to have an approximate solution for this case as the T-matrix method becomes less and less robust as the ratio d/R_c becomes smaller. For simplicity we shall not solve the problem inside the cloud, but we approximate its boundary as a pressure-release surface. It has been shown in Prosperetti *et al.* (1993) that, for the frequency range considered here, this procedure yields useful results already at gas volume fractions of the order of 1%.

We again start from the representation (3) of the pressure field but now we determine the scattered component approximately by requiring that it be a solution of the Helmholtz equation subject, on the plane $z=0$, to the condition

$$p^{\text{scat}}=F(\mathbf{x}_\parallel)\frac{\partial}{\partial z}(p^{\text{inc}}+p^{\text{ref}})\bigg|_{z=0}, \tag{52}$$

where $\mathbf{x}_\parallel \equiv (x,y)$ is the two-dimensional position vector in the plane undisturbed surface and

$$z=-F(\mathbf{x}_\parallel), \tag{53}$$

is the boundary of the cloud below the free surface. The condition (52) arises by satisfying approximately the pressure-release requirement $p=0$ on the surface (53).

The problem posed can readily be solved by use of the Green's function (46) to find the far-field result

$$p^{\text{scat}}\to -\frac{\exp(-ik|\mathbf{x}|)}{|\mathbf{x}|}\frac{k\mathbf{k}_\perp\cdot\mathbf{n}}{\pi}\int_A F(\mathbf{x}'_\parallel)\times\exp(ik\mathbf{x}'_\parallel\cdot\mathbf{n}-i\mathbf{k}_\parallel\cdot\mathbf{x}'_\parallel)dA', \tag{54}$$

where $\mathbf{n}=\mathbf{x}/|\mathbf{x}|$ is the unit vector in the direction of observation, $\mathbf{k}_\perp$ and $\mathbf{k}_\parallel$ are the components of $\mathbf{k}$ normal and parallel to the free surface, and the integral is over the footprint A of the cloud on the surface. Upon defining the dimensionless scattering amplitude f_* as in (12), where now R_c may be taken as the radius of the circle having the same area as the footprint of the cloud on the undisturbed free surface, we find

$$f_*=-\frac{k\mathbf{k}_\perp\cdot\mathbf{n}}{\pi R_c}\int_A F(\mathbf{x}'_\parallel)\exp(ik\mathbf{x}'_\parallel\cdot\mathbf{n}-i\mathbf{k}_\parallel\cdot\mathbf{x}'_\parallel)dA', \tag{55}$$

The low-frequency approximation $k|\mathbf{x}_\parallel|\to 0$ readily gives

$$f_*\simeq -\frac{k\mathbf{k}_\perp\cdot\mathbf{n}}{\pi R_c}\mathscr{V}, \tag{56}$$

where $\mathscr{V}$ is the volume of the cloud. It is clear from this result that f_* is proportional to the *first*, rather than third, power of the depth d of the cloud. Since d is small by assumption, this circumstance indicates a much stronger effect than predicted by the Born approximation. Clearly this is not a contradiction as, in the present case, the difference in the wave numbers inside and outside the cloud—on the smallness of which the Born approximation is predicated—is quite large.

As an example consider a cloud having the shape of an ellipsoid with semi-axes g and h ($g\geqslant h$) on the surface and semi-axis d in the vertical direction. As in Sec. II the plane of incidence is the (x,z) plane and the angle between the ellipsoid's minor semi-axis h and the x axis is denoted by γ. A simple calculation gives

$$f_*=\frac{2k^2\sin\eta\cos\theta\, dR_c}{\xi^3}(\xi\cos\xi-\sin\xi), \tag{57}$$

where

$$\xi=k\{g^2[\sin\theta\sin(\varphi-\gamma)+\cos\eta\sin\gamma]^2+h^2[\sin\theta\cos(\varphi-\gamma)-\cos\eta\cos\gamma]^2\}^{1/2}. \tag{58}$$

Here, as in Sec. II, the angles θ and φ are the polar coordinates of the observer referred to a system centered at the center of the ellipsoid. For the case of a spheroid $g=h=R_c$ and the previous expression becomes

$$\xi=kR_c[\sin^2\theta+\cos^2\eta-2\cos\eta\sin\theta\cos\varphi]^{1/2}. \tag{59}$$

Finally, for backscattering, $\theta=\frac{1}{2}\pi+\eta$, $\varphi=\pi$, and (58), (59) reduce to

$$\xi=2k\cos\eta[g^2\sin^2\gamma+h^2\cos^2\gamma]^{1/2}, \tag{60}$$

and

$$\xi=2kR_c\cos\eta, \tag{61}$$

respectively. The dimensionless cross section is related to f_* as before by (13).

We show some numerical results as a function of frequency in Figs. 15 and 16 for a grazing angle $\eta=20°$, $d=0.1$ m, and $R_c(=\sqrt{gh})=0.5$ m. Figure 15 is for $g/h=2$ (i.e., $g=0.707$ m, $h=0.354$ m) and Fig. 16 for $g/h=4$ (i.e., $g=1$ m, $h=0.25$ m). In the figures the solid curve is for the spheroidal case $g=h$. The dotted line is for $\gamma=\pi/2$, the short-dashed lines for $\gamma=\pi/4$, and the long-dashed lines for $\gamma=0$.

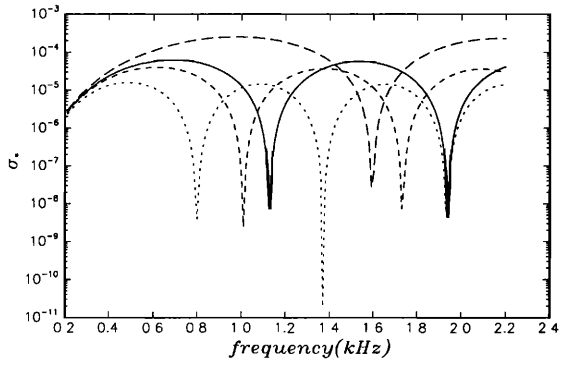

FIG. 15. Shallow approximation (57) for the dimensionless backscattering cross section from a pressure-release ellipsoidal "cloud." The axes of the footprint on the ocean's surface have dimensions $g=0.707$ m and $h=0.354$ m ($g/h=2$). The third axis, in the vertical downward direction, is $d=0.1$ m. The dotted line is for an angle γ between the projection of the incident wave vector on the horizontal plane and the minor horizontal axis of the ellipsoid equal to 0, the short-dashed line is for $\gamma=\pi/4$, and the long-dashed line for $\gamma=\pi/2$. The solid line is for the spheroidal case $g/h=1$. The grazing angle is 20°.

VIII. CONCLUSIONS

We have studied the effect of the shape of bubble clouds at the surface of an idealized plane ocean on the backscattering strength from the surface. This study complements the results reported earlier (Prosperetti *et al.*, 1993) where hemispherical clouds were treated in detail. Both studies have been based on a relatively simple model of bubbly liquid that has been found to be in excellent agreement with available data (Commander and Prosperetti, 1989; Lu *et al.*, 1990; Yoon *et al.*, 1991).

The conclusion of the present investigation is that the backscattering strength is but little affected by the detailed shape of the cloud. For all the cases considered, with reasonable assumptions on bubble population, cloud volume, and cloud surface coverage, we find backscattering levels in very good agreement with the Chapman and Harris (1962) experimental data. The effect of bubble clouds is quite strong. To fit the data for 10-m/s winds, for example, we only need clouds covering less than 1% of the ocean's surface, each occupying a volume of less than 1/3 m^3 and containing a total amount of gas of the order of 2 liters. Our findings therefore strongly support the suggestion that the unexpectedly high levels measured are due to the bubble clouds produced by breaking waves.

A similar conclusion has been reached in McDonald (1991) and Henyey (1991) where the backscattering strength of much more tenuous bubbly structures—so-called "plumes"—was studied. It is not possible in the light of the available evidence to discard one mechanism in favor of the other one and, indeed, it is quite possible that both clouds and plumes give contributions of comparable magnitude to the backscattering process. Experiments are required to discriminate between the two mechanisms and assess their relative importance. An experimental basis for such a distinction could conceivably be found in the fact that plumes are long-lived structures, while clouds are highly transient ones. Furthermore clouds, being produced by breaking waves, would also be responsible for strong acoustic emission in addition to scattering. In an ideal field experiment one would irradiate in a pulsed mode a limited surface area of the ocean and monitor both visually and by passive sonar the local occurrence of wave breaking. If the mechanism studied here is important, one would expect a strong correlation between enhanced backscattering and acoustic emissions.

We have also examined the validity of the Born approximation used in McDonald (1991) and Henyey (1991) for the study of bubble plumes. We have found that, for the range of gas volume fractions considered in those studies, the approximation is probably justified. Large differences with exact results would however be found already at gas volume fractions as low as 10^{-2}%. Finally, in a short analysis of the limit of three-dimensional shallow clouds, we have found that, for moderate or large volume fractions, the intensity of the backscattering is much stronger than what the Born approximation would lead one to believe.

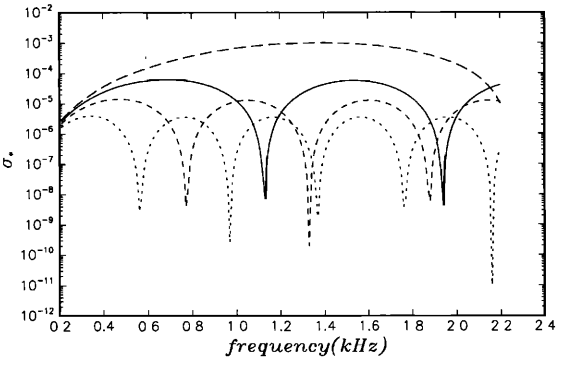

FIG. 16. Shallow approximation (57) for the dimensionless backscattering cross section from a pressure-release ellipsoidal "cloud." The axes of the footprint on the ocean's surface have dimensions $g=0.1$ m and $h=0.25$ m ($g/h=4$). The third axis, in the vertical downward direction, is $d=0.1$ m. The dotted line is for $\gamma=0$, the short-dashed line for $\gamma=\pi/4$, and the long-dashed line for $\gamma=\pi/2$. The solid line is for the spheroidal case $g/h=1$. The grazing angle is 20°.

ACKNOWLEDGMENT

This study has been supported by the Ocean Acoustics program of the Office of Naval Research.

Carey, W. M., and Bradley, M. P. (**1985**). "Low-frequency ocean surface noise sources," J. Acoust. Soc. Am. Suppl. 1 **78**, S1–S2.

Carey, W. M., and Browning, D. (**1988**). "Low-frequency ocean ambient noise: Measurement and theory," in *Sea Surface Sound*, edited by B. R. Kerman (Kluwer, Dordrecht), pp. 361–376.

Chapman, R. P., and Harris, J. H. (**1962**). "Surface backscattering strengths measured with explosive sound sources," J. Acoust. Soc. Am. **34**, 1592–1597.

Commander, K. W., and Prosperetti, A. (**1989**). "Linear pressure waves in bubbly liquids: comparison between theory and experiment," J. Acoust. Soc. Am. **85**, 732–746.

Crowther, P. A. (**1980**). "Acoustic scattering from near-surface bubble layers," in *Cavitation and Inhomogeneities in Underwater Acoustics*, edited by W. Lauterborn (Springer-Verlag, New York), pp. 194–204.

Henyey, F. S. (**1991**). "Acoustic scattering from oceanic microbubble plumes in the 100 Hz to 2 kHz region," J. Acoust. Soc. Am. **90**, 399–405.

Lu, N. Q., and Prosperetti, A. (**1993**). "Active and passive acoustic behavior of bubbly layers," J. Acoust. Soc. Am. (submitted).

Lu, N. Q., Prosperetti, A., and Yoon, S. W. (**1990**). "Underwater noise emissions from bubble clouds," IEEE J. Ocean. Eng. **15**, 275–281.

McDaniel, S. T. (**1988**). "Acoustical estimates of subsurface bubble densities in the open ocean and coastal waters," in *Sea Surface Sound*, edited by B. R. Kerman (Kluwer, Dordrecht), pp. 225–236.

McDaniel, S. T., and Gorman, A. D. (**1982**). "Acoustic and radar sea surface backscattering," J. Geophys. Res. **87**, 4127–4136.

McDonald, B. E. (**1991**). "Echoes from vertically striated subresonant bubble clouds: A model for ocean surface reverberation," J. Acoust. Soc. Am. **89**, 617–622.

Monahan, E. C., and O'Muircheartaigh, I. G. (**1980**). "Optimal power-law description of oceanic whitecap coverage dependence on wind speed," J. Phys. Oceanogr. **10**, 2094–2099.

Nicholas, M., Roy, R. A., Crum, L. A., Oğuz, H. N., and Prosperetti, A. (**1993**). "Sound emission by a laboratory bubble cloud," J. Acoust. Soc. Am. (submitted).

Prosperetti, A. (**1985**). "Bubble-related ambient noise in the ocean," J. Acoust. Soc. Am. Suppl. 1 **78**, S2.

Prosperetti, A. (**1988a**). "Bubble dynamics in oceanic ambient noise," in *Sea Surface Sound*, edited by B. R. Kerman (Kluwer, Dordrecht), pp. 151–171.

Prosperetti, A. (**1988b**). "Bubble-related ambient noise in the ocean," J. Acoust. Soc. Am. **84**, 1042–1054.

Prosperetti, A., Lu, N. Q., and Kim, H. S. (**1993**). "Active and passive behavior of bubble clouds at the ocean's surface," J. Acoust. Soc. Am. **93**, 3117–3127.

Sarkar, K., and Prosperetti, A. (**1993**). "Incoherent scattering due to bubbles," J. Acoust. Soc. Am. (submitted).

Urick, R. J. (**1967**), *Principles of Underwater Sound for Engineers* (McGraw-Hill, New York), Chap. 8, p. 188.

Visscher, W. M. (**1980a**). "A new way to calculate scattering of acoustic and elastic waves I. Theory illustrated for scaler waves," J. Appl. Phys. **51**, 825–834.

Visscher, W. M. (**1980b**). "A new way to calculate scattering of acoustic and elastic waves II. Application to elastic waves scattered from voids and fixed rigid obstacles," J. Appl. Phys. **51**, 835–845.

Waterman, P. C. (**1969**). "New formulation of acoustic scattering," J. Acoust. Soc. Am. **45**, 1417–1429.

Yeh, C. (**1967**). "Scattering of acoustic waves by a penetrable prolate spheroid. I. Liquid prolate spheroid," J. Acoust. Soc. Am. **42**, 518–521.

Yoon, S. W., Crum, L. A., Prosperetti, A., and Lu, N. Q. (**1991**), "An investigation of the collective oscillations of a bubble cloud," J. Acoust. Soc. Am. **89**, 700–706.